

# Excited Leptonic States in Polarized $e^-\gamma$ and $e^+e^-$ Collisions

O. J. P. Éboli

*Instituto de Física, Universidade de São Paulo,*

*C.P. 66318, 05389-970 São Paulo, Brazil*

E. M. Gregores, J. C. Montero, S. F. Novaes, and D. Spehler

*Instituto de Física Teórica, Universidade Estadual Paulista*

*Rua Pamplona 145, 01405-900 São Paulo, Brazil*

## Abstract

We analyze the capability of the next generation of linear electron–positron colliders to unravel the spin and couplings of excited leptons predicted by composite models. Assuming that these machines will be able to operate both in the  $e^+e^-$  and  $e^-\gamma$  modes, we study the effects of the excited electrons of spin  $\frac{1}{2}$  and  $\frac{3}{2}$  in the reactions  $e^-\gamma \rightarrow e^-\gamma$  and  $e^+e^- \rightarrow \gamma\gamma$ . We show how the use of polarized beams is able not only to increase the reach of these machines, but also to determine the spin and couplings of the excited states.

12.60.Rc, 14.60.Hi, 13.88.+e

## I. INTRODUCTION

The standard model (SM) of the electroweak interactions explains extremely well all the available experimental data [1]. Notwithstanding, it has some unpleasant features, such as the large number of free parameters, the proliferation of fermionic generations, and their complex pattern of masses and mixing angles. A rather natural explanation for the existence of the fermionic generations is that the known leptons and quarks are composite [2], sharing some common constituents (preons). In this sense, it is conceivable that the SM is just the low energy limit of a more fundamental theory, which is characterized by a large mass scale  $\Lambda$ . In general, composite models exhibit a rich spectrum which includes many new states like the excitations of the known particles.

Since the existence of excited fermions is an undeniable signal for new physics beyond the SM, there have been several direct searches for these particles at different accelerators. At the CERN Large Electron–Positron Collider (LEP), the experiments excluded the existence of excited spin- $\frac{1}{2}$  fermions with mass up to 46 GeV from the pair production search, and up to 90 GeV from direct single production for a scale of compositeness  $\Lambda < 2.5$  TeV [3]. Moreover, a limit on the mass of an excited electron of  $M_{e^*} > 127$  GeV at 95% of confidence level was set from the measurement of the  $e^+e^- \rightarrow \gamma\gamma$  cross section [3]. On the other hand, the experiments at the DESY  $ep$  collider HERA searched, in a model independent way, for resonances in the  $e\gamma$ ,  $\nu W$ , and  $eZ$  systems [4], however the LEP bounds on excited leptons couplings are about one order of magnitude more stringent in the mass region just below the  $Z$  mass.

Up to now all the direct searches for compositeness have failed, and we expect that the next generation of accelerators, working at higher center-of-mass energies, will be able to further extend the search for composite states. On the theoretical side, there have been extensive studies on the possibility of unraveling the existence of excited fermions in  $pp$  [5,6],  $e^+e^-$  [6–10], and  $ep$  [8,9] collisions at higher energies.

A particularly interesting machine for analyzing the substructure of the electron and its

neutrino is the Next Linear  $e^+e^-$  Collider (NLC) that is been planned to operate with a center-of-mass energy of at least 500 GeV and an integrated luminosity around  $10 \text{ fb}^{-1}$  [11]. At the NLC, it will be possible to convert an electron beam into a photon one focusing a laser on the electron beam. By Compton scattering, high energy photons are produced along the electron direction carrying away a large amount of the beam energy [12,13]. The laser backscattering mechanism will allow the NLC to operate in three different modes,  $e^+e^-$ ,  $e^-\gamma$ , and  $\gamma\gamma$ , opening up an opportunity for a deeper search for compositeness [9,10]. A nice feature of the  $e^-\gamma$  mode of NLC is the possibility of searching for new excited charged leptons as resonances in the  $e^-\gamma$  scattering [10].

In this work we analyze the deviations from the SM predictions of the reactions  $e^-\gamma \rightarrow e^-\gamma$  and  $e^+e^- \rightarrow \gamma\gamma$  due to the exchange of excited spin- $\frac{1}{2}$  and spin- $\frac{3}{2}$  fermions. In particular, it is important to determine the spin of the fermionic excitations since the allowed values of the spin can give hints about the underlying preonic structure [6]. We perform a detailed study of the experimental signatures of excited fermions exploring the possibility of polarizing both the electron and laser beams, and we point out the best strategy to unravel the spin and the chiral couplings of the excited leptons to the usual particles. We also study the discovery limits on the new physics parameters and we show that an  $e^-\gamma$  collider can probe very large values of the compositeness scale ( $\Lambda$ ), *e.g.* for excited electron masses of the order of 400 GeV we can explore up to  $\Lambda \sim 200$  TeV.

The outline of this paper is the following. In Sec. II, we introduce the effective Lagrangians describing the excited fermion couplings and discuss the existing low energy constraints. The analysis of the reaction  $e^-\gamma \rightarrow e^-\gamma$  is contained in Sec. III, where we also present the main ingredients of the laser backscattering mechanism. Section IV exhibits the study of the reaction  $e^+e^- \rightarrow \gamma\gamma$  for LEP II and NLC energies and our results are summarized in Sec. V. This paper is supplemented with an appendix that contains the complete helicity amplitudes for the processes under study, as well as for the decays of the excited leptons.

## II. EFFECTIVE LAGRANGIANS

Composite models cannot be analyzed perturbatively since the preons interact strongly at the energy scales of interest. Instead, we must rely on effective Lagrangians to describe the couplings of excited states with ordinary fermions and vector bosons. We demanded that the effective Lagrangians for the excited fermions are  $CP$  conserving and that they respect the  $U(1)_{\text{em}}$  gauge invariance. We considered a magnetic moment type coupling among the excited spin- $\frac{1}{2}$  fermion ( $\Psi_{1/2}^*$ ), the ground state fermion ( $\psi$ ), and the photon that is described by the effective Lagrangian [14–16]

$$\mathcal{L}_{\text{eff}}^{1/2} = \frac{e}{2\Lambda} \bar{\Psi}_{1/2}^* \sigma^{\mu\nu} (A + B\gamma_5) \psi F_{\mu\nu} + \text{h.c.} , \quad (1)$$

where  $\Lambda$  is the compositeness scale and  $F_{\mu\nu}$  is the electromagnetic field strength tensor. For the coupling of spin- $\frac{3}{2}$  excited states ( $\Psi_{3/2}^{*\mu}$ ) to usual fermions and photons, we adopted the lowest order  $U(1)_{\text{em}}$  gauge-invariant effective Lagrangian that can be constructed out of these fields [6,17,18]

$$\mathcal{L}_{\text{eff}}^{3/2} = \frac{e}{\Lambda} \bar{\Psi}_{3/2}^{*\mu} \gamma^\nu (C + D\gamma_5) \psi F_{\mu\nu} + \text{h.c.} , \quad (2)$$

where  $\sigma_{\mu\nu} = \frac{i}{2}[\gamma_\mu, \gamma_\nu]$ . The constants  $A$ ,  $B$ ,  $C$ , and  $D$  are assumed to be real in order to preserve CP invariance. In general, the effective Lagrangians (1) and (2) can be embodied in a wider class of models [8] that respects the  $SU(2)_L \times U(1)_Y$  gauge invariance, provided that the couplings are chosen conveniently. Since we are interested only in electromagnetic transitions, we ignored the possible coupling of the excited states with the weak gauge bosons in the present work.

The above couplings of the excited leptons allow them to decay predominantly into the ground state lepton through the emission of a photon with widths

$$\begin{aligned} \Gamma_{1/2} &\simeq \Gamma_{1/2}(L_{1/2} \rightarrow e\gamma) = \frac{\alpha M_{1/2}^3}{\Lambda^2} , \\ \Gamma_{3/2} &\simeq \Gamma_{3/2}(L_{3/2} \rightarrow e\gamma) = \frac{\alpha M_{3/2}^3}{4\Lambda^2} . \end{aligned} \quad (3)$$

In this work, we assumed that the branching ratio of these particles into electron–photon pairs is equal to one. The helicity amplitudes for these decays are presented in the Appendix.

The above Lagrangians are constrained by the direct searches in collider experiments, as well as by their effect in the low–energy phenomenology. Excited fermions can contribute to atomic parity violation, electron–deuteron scattering [19], and the anomalous magnetic moment of leptons ( $e$  and  $\mu$ ) [14,20]. For an arbitrary choice of the couplings  $A$ ,  $B$ ,  $C$ , and  $D$  the most stringent bounds on excited fermions are due to their contribution to the  $(g-2)$  of the muon. However, these limits can be softened if we consider only chiral couplings, *i.e.* the new interactions have either a right–handed (RH) or left–handed (LH) structure [14]. In this case the contributions of the spin– $\frac{1}{2}$  and spin– $\frac{3}{2}$  excited states to  $(g-2)$  is proportional to  $m_\mu^2/\Lambda^2$ , and the bound reads  $\Lambda \gtrsim 800$  GeV. In our numerical results, we have taken into account the experimental LEP bound on the mass and coupling of the excited fermions and also the bound coming from the very precise measurement of anomalous magnetic moments.

### III. ELECTRON–PHOTON COLLISIONS

#### A. Polarized Laser Backscattering Distribution Functions and Cross Sections

In a linear collider it is possible to transform an electron (positron) beam into a intense  $\gamma$  one through the process of laser backscattering [12]. This mechanism relies on the fact that Compton scattering of energetic electrons by soft laser photons gives rise to high energy photons, that are collimated in the direction of the incident electron. Another very powerful feature of the Compton backscattering mechanism is the possibility of obtaining a high degree of polarization for the backscattered photons by polarizing the incoming electron and (or) laser beams. The backscattered photon distribution function for polarized electron and laser beams is [13]

$$F(x, \zeta; P_e, P_l) = \frac{2\pi\alpha^2}{\zeta m^2 \sigma_c} \left[ \frac{1}{1-x} + 1 - x - 4r(1-r) - P_e P_l r \zeta (2r-1)(2-x) \right], \quad (4)$$

where  $P_e$  is the mean parent electron longitudinal polarization,  $P_l$  represents the laser photon circular polarization, and  $\sigma_c$  is the Compton cross section

$$\sigma_c = \sigma_c^0 + P_e P_l \sigma_c^1 , \quad (5)$$

with

$$\begin{aligned} \sigma_c^0 &= \frac{2\pi\alpha^2}{\zeta m^2} \left[ \left( 1 - \frac{4}{\zeta} - \frac{8}{\zeta^2} \right) \ln(\zeta + 1) + \frac{1}{2} + \frac{8}{\zeta} - \frac{1}{2(\zeta + 1)^2} \right] , \\ \sigma_c^1 &= \frac{2\pi\alpha^2}{\zeta m^2} \left[ \left( 1 + \frac{2}{\zeta} \right) \ln(\zeta + 1) - \frac{5}{2} + \frac{1}{\zeta + 1} - \frac{1}{2(\zeta + 1)^2} \right] . \end{aligned} \quad (6)$$

We defined the variables

$$x = \frac{\omega}{E} , \quad \zeta = \frac{4E\omega_0}{m^2} , \quad r = \frac{x}{\zeta(1-x)} , \quad (7)$$

where  $m$  and  $E$  are the electron mass and energy,  $\omega_0$  is the laser energy, and  $\omega$  is the backscattered photon energy. The variable  $x \leq x_{\max} \equiv \zeta/(\zeta + 1)$  represents the fraction of the electron energy carried by the backscattered photon and  $r \leq 1$ . In our calculations, we assumed  $\zeta = 2(1 + \sqrt{2}) \simeq 4.83$  in order to maximize the backscattered photon energy without spoiling the luminosity through  $e^+e^-$  pair creation by the interaction between laser and backscattered photons.

The backscattered photon spectrum (4) depends only upon the product  $P_e P_l$ , and the unpolarized distribution is recovered if either the electron beam or the laser is not polarized. As can be seen from Fig. 1a, for negative values of this product the spectrum is dominated by hard photons, otherwise it is quite broad. We should notice that for  $r = 1/2$  the distribution function (4) depends on the electron and laser polarization only through  $\sigma_c$  and the distribution functions, for any electron and laser polarization, have approximately the same value at  $x = \zeta/(\zeta + 2) \simeq 0.71$ .

The mean backscattered photon helicity is given by the Stokes parameter

$$\xi_2 = \frac{P_e r \zeta \left[ 1 + (1-x)(2r-1)^2 \right] - P_l (2r-1) [1/(1-x) + 1-x]}{1/(1-x) + 1-x - 4r(1-r) - P_e P_l r \zeta (2r-1)(2-x)} . \quad (8)$$

For  $x = x_{\max}$  (or  $r = 1$ ) and  $P_e = 0$  or  $P_l = \pm 1$ , we have  $\xi_2 = -P_l$ , *i.e.* the polarization of the backscattered photon beam has the opposite value of the laser polarization. Moreover, for  $x = \zeta/(\zeta + 2)$  (or  $r = 1/2$ ), the Stokes parameter  $\xi_2$  is independent of the laser polarization (see Fig. 1b) and is given by

$$\xi_2^{(r=1/2)} = P_e \frac{\zeta(\zeta + 2)}{\zeta(\zeta + 2) + 4} . \quad (9)$$

The cross section for the reaction  $e^- \gamma \rightarrow X$  in a  $e^+e^-$  linear collider, where the positron beam with longitudinal polarization  $P_p$  is converted into a backscattered photon beam, is

$$d\sigma_{P_e \xi_2} (e^- \gamma \rightarrow X) = \kappa \int_{x_{\min}}^{x_{\max}} dx F(x, \zeta; P_p, P_l) d\hat{\sigma}_{P_e \xi_2}(e\gamma \rightarrow X) , \quad (10)$$

where  $\kappa$  is the efficiency of the laser backscattering mechanism [21], that we assumed to be one, and  $d\hat{\sigma}_{P_e \xi_2}$  is the polarized cross section for the subprocess  $e^- \gamma \rightarrow X$  which depends on  $\hat{s} = xs$ . In general, this polarized cross section can be written as

$$d\hat{\sigma}_{P_e \xi_2} = \frac{1}{4} \left[ (1 + P_e \xi_2) (d\hat{\sigma}_{++} + d\hat{\sigma}_{--}) + (P_e + \xi_2) (d\hat{\sigma}_{++} - d\hat{\sigma}_{--}) + (1 - P_e \xi_2) (d\hat{\sigma}_{+-} + d\hat{\sigma}_{-+}) + (P_e - \xi_2) (d\hat{\sigma}_{+-} - d\hat{\sigma}_{-+}) \right] , \quad (11)$$

with  $d\hat{\sigma}_{\lambda_e \lambda_\gamma}$  ( $\lambda_{e(\gamma)} = \pm 1$ ) being the polarized subprocess cross section for full electron and photon polarizations,  $P_e$  is the longitudinal polarization of the electron beam, and  $\xi_2$  is given by Eq. (8).

## B. Results

The complete set of the helicity amplitudes for the subprocess

$$e^- \gamma \rightarrow (e^-, L_{1/2(3/2)}^-) \rightarrow e^- \gamma , \quad (12)$$

are presented in the Appendix for the exchange of spin- $\frac{1}{2}$  (A6) and spin- $\frac{3}{2}$  (A7) excited fermions in the  $s$ -channel. In order to avoid the strong bounds coming from the muon ( $g - 2$ ) measurements, we assumed either left-handed (LH) ( $A = -B = 1$  and  $C = -D = 1$ )

or right-handed (RH) ( $A = B = 1$  and  $C = D = 1$ ) couplings. In order to quantify the potential of an  $e^- \gamma$  collider to search for excited states, we defined the statistical significance of the signal ( $\mathcal{S}$ ) by

$$\mathcal{S} \equiv \frac{|\sigma_{\text{exc}} - \sigma_{\text{QED}}|}{\sqrt{\sigma_{\text{QED}}}} \sqrt{\mathcal{L}} , \quad (13)$$

where  $\sigma_{\text{exc}}$  ( $\sigma_{\text{QED}}$ ) is the cross section associated to the excited lepton (QED) contributions and  $\mathcal{L}$  is the integrated luminosity of the machine.

The existence of an excited fermion with mass below the kinematical reach of the  $e^- \gamma$  machine can be established through the identification of its Breit–Wigner profile in the  $e^- \gamma$  invariant mass distribution ( $M$ ), which should be an easy task even in the case of unpolarized beams. We present in Fig. 2 the distribution  $d\sigma/dM$  for  $M_{1/2(3/2)} = 250$  GeV at an  $e^+e^-$  collider with  $\sqrt{s} = 500$  GeV, where we introduced a cut in the polar angle ( $\theta$ ) of the final state particles with the beam pipe requiring that  $5^\circ < \theta < 175^\circ$ . For the sake of comparison, we plotted this distribution for QED (*i.e.*  $\Lambda = \infty$ ) and for values of the compositeness scale that lead to a  $3\sigma$  effect in the total cross section.

The search for excited leptons certainly can be conducted using unpolarized beams, however, polarization can be used not only to expand the discovery region in the  $\Lambda \times M_{1/2(3/2)}$  plane, through the enhancement of the luminosity and the cross section, but also to study in detail the interaction of the new states. As we pointed out before, the distribution functions assume approximately the same value at  $\bar{x} = \zeta/(\zeta+2) \simeq 0.71$ , even for different polarization configurations of the initial particles. In the interval  $0 < x < \bar{x}$ , the luminosity is higher for  $P_p P_l > 0$ , whereas for the range  $x > \bar{x}$  the distribution with  $P_p P_l < 0$  dominates. Therefore, in order to search for excited leptons with mass below (above)  $\bar{M} = \sqrt{\bar{x}s}$ , we should employ the polarization configurations of the electron and the laser in such a way that  $P_p P_l > 0$  ( $< 0$ ). In both cases, the degree of circular polarization of the scattered photon ( $\xi_2$ ) has the same sign as the positron polarization in the region of interest. Moreover, we can see from the helicity amplitudes presented in the Appendix that  $\xi_2 > 0$  enhances the cross section for RH spin- $\frac{1}{2}$  and LH spin- $\frac{3}{2}$  excited states, while  $\xi_2 < 0$  favors those with

LH spin- $\frac{1}{2}$  and RH spin- $\frac{3}{2}$ . This behavior can be easily traced to the angular momenta configuration of the initial state.

Keeping the above comments in mind, we can envisage four different scenarios to enlarge the discovery region in the  $\Lambda \times M_{1/2(3/2)}$  plane, depending on the spin, mass, and couplings of the excited fermion:

- (i)  $P_p > 0$  and  $P_l > 0$  for RH spin- $\frac{1}{2}$  or LH spin- $\frac{3}{2}$  excited states with mass below  $\overline{M}$ ;
- (ii)  $P_p < 0$  and  $P_l < 0$  for LH spin- $\frac{1}{2}$  or RH spin- $\frac{3}{2}$  excited states with mass below  $\overline{M}$ ;
- (iii)  $P_p < 0$  and  $P_l > 0$  for LH spin- $\frac{1}{2}$  or RH spin- $\frac{3}{2}$  excited states with mass above  $\overline{M}$ ;
- (iv)  $P_p > 0$  and  $P_l < 0$  for RH spin- $\frac{1}{2}$  or LH spin- $\frac{3}{2}$  excited states with mass above  $\overline{M}$ .

Besides the above procedure, we can also increase the excited fermion cross section by polarizing the electron beam. In fact, we can learn from the expressions for the subprocess cross section given in the Appendix, that the use of negatively (positively) polarized electrons enhances the signal for excited states with LH (RH) couplings, as is naively expected. In general, polarized electron beams increase the sensitivity to  $\Lambda$  by a factor 2–3 for a given value of  $M_{1/2(3/2)}$ .

Figs. 3a and 3b show the discovery region for several polarizations of the initial particles, where the region that can be accessed at the NLC is located below and to the left of the curves. For excited electron masses lower than the kinematical limit of the  $e^- \gamma$  collider, we required a  $3\sigma$  effect in the cross section obtained by the integration over a bin of 5 GeV around the excited lepton mass. We also introduced the angular cut  $5^\circ < \theta < 175^\circ$ , that mimics the angular coverage of a detector and also reduces the size of the QED background. For masses larger than the kinematical limit of the collider, we evaluated  $\mathcal{S}$  using the total cross section. We can learn from these figures that electron–photon collisions are able to explore very large values of the compositeness scale, extending considerably the limits currently available from low energy experiments. For instance, in the case of an excited spin- $\frac{1}{2}$  lepton with mass around 400 GeV we can probe up to  $\Lambda \sim 200$  TeV.

Once the existence of excited electrons is established, it is important to study its spin and couplings. At this point the use of polarized beams is crucial to determine the properties

of the excited fermion. In order to unravel the hardness of the excited electron coupling, we studied the cross section (10) when only the electron beam is polarized. In this case, we can write

$$\sigma = \sigma_{00} (1 + P_e \mathcal{A}_{LR}) , \quad (14)$$

where  $\sigma_{00}$  stands for the cross section for unpolarized beams and  $\mathcal{A}_{LR}$  is the left-right asymmetry factor

$$\mathcal{A}_{LR} = \frac{\sigma_R - \sigma_L}{\sigma_R + \sigma_L} , \quad (15)$$

with  $\sigma_{R(L)}$  being the cross section for fully polarized electron beams and unpolarized backscattered photons.

In Fig. 4a we exhibit the deviation

$$\delta_e = \frac{\sigma_{e0} - \sigma_{00}}{\sigma_{00}} \quad (16)$$

of the polarized cross section ( $\sigma_{e0}$ ) with respect to the unpolarized one ( $\sigma_{00}$ ), as function of the excited state mass. Our results were obtained integrating the cross sections over a 5 GeV bin around the resonance and assuming that the electron beam has a degree of longitudinal polarization of 90%. We required that the total number of events, for the polarized case, differs by  $3\sigma$  from the unpolarized yield. From this figure, we can witness that the measurement of such a deviation is capable of distinguishing very clearly RH from LH couplings, as it is expected from naive arguments. Moreover, the left-right asymmetry can also be inferred, in a straightforward way, from this measurement. Notwithstanding, we can not discriminate between excited fermions of spin  $\frac{1}{2}$  and  $\frac{3}{2}$  by the analysis of this deviation only. This task can be accomplished by studying the same process with polarized photon beams.

In fact, as we have pointed above,  $\xi_2 > 0$  enhances the cross section for RH spin- $\frac{1}{2}$  and LH spin- $\frac{3}{2}$  excited states, while  $\xi_2 < 0$  favors LH spin- $\frac{1}{2}$  and RH spin- $\frac{3}{2}$  excited states. Therefore, we defined the deviation

$$\delta_\gamma = \frac{\sigma_{0\gamma} - \sigma_{00}}{\sigma_{00}}, \quad (17)$$

where  $\sigma_{00}$  is the unpolarized cross section and  $\sigma_{0\gamma}$  is the cross section integrated over the 5 GeV bin around the resonance for polarized backscattered photons and unpolarized electrons. In this case, we cannot define an asymmetry factor, in the same way we did before, since  $\xi_2$  is a function of the momentum carried by the photon (see Eq. (8)).

We present in Fig. 4b the deviation  $\delta_\gamma$  as a function of the excited state mass, requiring that the total number of events of the polarized case differs by  $3\sigma$  from the unpolarized one. In order to obtain the polarized backscattered photons, we assumed that the parent positron beam has a 90% degree of polarization and that the laser beam is not polarized. In this setup, the polarization of the backscattered photon ( $\xi_2$ ) has the same sign of the parent positron polarization for the whole spectrum. From this figure, we verify that RH spin- $\frac{1}{2}$  and LH spin- $\frac{3}{2}$  fermions lead to positive values of this deviation, whereas LH spin- $\frac{1}{2}$  and RH spin- $\frac{3}{2}$  fermions furnish negative values for it [22]. Therefore, once the handness of the coupling is established through the analysis of  $\delta_e$  the spin of the resonance can be determined by measuring  $\delta_\gamma$ .

#### IV. ELECTRON-POSITRON COLLISIONS

We learned in the previous section that an  $e^-\gamma$  collider is a powerful tool to investigate the existence of excited fermions with mass below the kinematical reach of the machine. For masses above this limit, it is worthwhile to employ the  $e^+e^-$  mode of the collider, since excited fermions appear as a virtual state being exchanged on the  $t$ -channel of the process  $e^+e^- \rightarrow \gamma\gamma$ .

The polarized cross section for this process is given by

$$d\sigma_{P_e P_p} = \frac{1}{4} \left[ (1 + P_p P_e) (d\sigma_{++} + d\sigma_{--}) + (P_p + P_e) (d\sigma_{++} - d\sigma_{--}) + (1 - P_p P_e) (d\sigma_{+-} + d\sigma_{-+}) + (P_p - P_e) (d\sigma_{+-} - d\sigma_{-+}) \right], \quad (18)$$

where  $P_{e(p)}$  is the electron (positron) mean longitudinal polarization and  $d\sigma_{\lambda_p \lambda_e}$ , with  $\lambda_{p(e)} =$

$\pm 1$ , is the cross section for fully polarized  $e^+$  and  $e^-$  beams. For completeness, the helicity amplitudes for the exchange of a spin- $\frac{1}{2}$  (A8) and a spin- $\frac{3}{2}$  (A9) excited electron are presented in the Appendix.

For the sake of comparison, Fig. 5 contains the angular distribution of the produced photons in  $e^+e^- \rightarrow \gamma\gamma$  for QED and excited leptons of spin  $\frac{1}{2}$  and  $\frac{3}{2}$ . The lines in this figure correspond to couplings that lead to a  $3\sigma$  deviation from the QED total cross section. As we could expect, unpolarized beams cannot be used to determine the chirality of the coupling of the excited electron. Moreover, only a detailed experimental study of the angular distribution of the two photons could, in principle, distinguish between a spin- $\frac{1}{2}$  and a spin- $\frac{3}{2}$  new fermion contribution.

Since polarization increases or reduces the total cross section according to the chirality of the couplings, the distinction between RH and LH couplings can be made very easily by polarizing just the electron beam. In this case, we can compute the left-right asymmetry  $\mathcal{A}_{LR}$  aforementioned. In Fig. 6, we show  $\mathcal{A}_{LR}$  as function of  $M_{1/2(3/2)}$  for  $\Lambda = 1$  TeV. Notice that the chirality nature of the excited state can be clearly discerned by looking at the sign of this asymmetry.

We present in Fig. 7 the discovery limits obtained from this reaction for unpolarized beams at the LEP II energies. We considered two different sets of parameters for this collider, *i.e.*  $\sqrt{s} = 175$  GeV with  $\mathcal{L} = 500 \text{ pb}^{-1}$  and  $\sqrt{s} = 205$  GeV with  $\mathcal{L} = 300 \text{ pb}^{-1}$ . We required a  $3\sigma$  effect in the total cross section for the  $\gamma\gamma$  production and imposed a cut of  $12^\circ$  in the polar angle of the final photons with the beam pipe. We can see from this simulation that the discovery region is larger for the  $\sqrt{s} = 175$  GeV and  $\mathcal{L} = 500 \text{ pb}^{-1}$  operation mode, no matter the spin of the excited state. As expected, both LH and RH couplings give the same result.

Finally, we compare in Fig. 8a (8b) the discovery regions of spin- $\frac{1}{2}(\frac{3}{2})$  excited states for the machine operating in the  $e^-\gamma$  and  $e^+e^-$  modes. We considered  $3\sigma$  deviations in the total cross section and assumed unpolarized beams, performing a  $5^\circ$  cut on the polar angle to avoid the beam pipe region. As we can see from these figures, the  $e^-\gamma$  operating mode is

by far more advantageous to investigate the existence of such states even when their masses are larger than the center-of-mass energy of the machine.

## V. CONCLUSION

The existence of excited fermions is a direct consequence of a possible new layer of matter. In this paper we have analyzed the capability of an  $e^+e^-$  machine, operating both in  $e^+e^-$  and  $e^-\gamma$  modes, to discover and study such new states. Using polarized beams, we showed how to determine whether the spin of the excited state is  $\frac{1}{2}$  or  $\frac{3}{2}$  and also the chiral structure of its coupling to photons and usual fermions.

We showed that  $e^-\gamma$  reaction is the best way to search for excited electrons even for masses above the kinematical reach of the machine. Moreover, in these collisions, an important rôle is played by the polarization of the beams since it allows the identification of the chiral structure of the excited state coupling through the measurement of deviations from the unpolarized cross section, when only the electron beam is polarized. The identification of its spin can be done in the  $e^-\gamma$  mode when, in addition to the measurement of such deviation, a second measurement is made employing just a polarized photon beam. We have also showed in the  $\Lambda \times M_{1/2(3/2)}$  plane how the use of polarized beams can enlarge in a significant way the reach of these machines.

## ACKNOWLEDGMENTS

This work was partially supported by Conselho Nacional de Desenvolvimento Científico e Tecnológico (CNPq) and by Fundação de Amparo à Pesquisa do Estado de São Paulo (FAPESP).

## APPENDIX:

In this appendix we present the helicity amplitudes for the decay  $L_{1/2(3/2)}^- \rightarrow e^- \gamma$  and for the processes  $e^- \gamma \rightarrow (e^-, L_{1/2(3/2)}^-) \rightarrow e^- \gamma$  and  $e^+ e^- \rightarrow \gamma \gamma$ , considering the couplings described by the Lagrangians (1) and (2). In order to evaluate these helicity amplitudes we used the Weyl–van der Waerden spinor technique for spin- $\frac{1}{2}$  [23] and spin- $\frac{3}{2}$  [24] fermions. In this formalism the usual propagator of spin- $\frac{3}{2}$  fermions

$$P^{\mu\nu}(k) = \frac{k + M_{3/2}}{k^2 - M_{3/2}^2} \left[ -g^{\mu\nu} + \frac{1}{3} \gamma^\mu \gamma^\nu + \frac{1}{3M_{3/2}^2} (k \gamma^\mu k^\nu + \gamma^\nu k^\mu k^\nu) \right],$$

can be written in spinorial notation as [25]

$$P^{\mu\nu}(k) = \frac{1}{\frac{1}{2}\{K, \bar{K}\} - M_{3/2}^2} \begin{pmatrix} M_{3/2} \delta_p^b (A_{d\dot{e}f\dot{g}})_b^c & K_{a\dot{b}} (B_{d\dot{e}f\dot{g}})_{\dot{b}}^{\dot{c}} \\ \bar{K}^{\dot{a}b} (A_{d\dot{e}f\dot{g}})_b^c & M_{3/2} \delta_{\dot{b}}^{\dot{a}} (B_{d\dot{e}f\dot{g}})_{\dot{b}}^{\dot{c}} \end{pmatrix} \sigma^{\mu d\dot{e}} \bar{\sigma}^{\nu f\dot{g}}, \quad (A1)$$

where

$$\begin{aligned} (A_{d\dot{e}f\dot{g}})_b^c &= -\frac{1}{2} \delta_b^c \epsilon_{dg} \epsilon_{\dot{e}\dot{f}} - \frac{1}{3} \delta_g^c \epsilon_{bd} \epsilon_{\dot{e}\dot{f}} + \frac{1}{6M_{3/2}^2} (\delta_d^c K_{b\dot{e}} K_{g\dot{f}} - \epsilon_{bg} K_{d\dot{e}} K_{\dot{f}}^c), \\ (B_{d\dot{e}f\dot{g}})_{\dot{b}}^{\dot{c}} &= -\frac{1}{2} \delta_{\dot{b}}^{\dot{c}} \epsilon_{dg} \epsilon_{\dot{e}\dot{f}} + \frac{1}{3} \delta_{\dot{e}}^{\dot{b}} \epsilon_{dg} \epsilon_{\dot{c}\dot{f}} + \frac{1}{6M_{3/2}^2} (\delta_{\dot{f}}^{\dot{b}} \bar{K}_{\dot{c}g} \bar{K}_{\dot{e}d} - \epsilon_{\dot{c}\dot{e}} \bar{K}_{\dot{d}}^{\dot{b}} \bar{K}_{\dot{f}g}). \end{aligned} \quad (A2)$$

In the decay  $L_{1/2(3/2)}^- \rightarrow e^- \gamma$  we denote the square of the helicity amplitudes for the decay of a spin- $\frac{1}{2}$  excited fermion by  $|\mathcal{M}_{\lambda_L; \lambda_e \lambda_\gamma}^{1/2}|^2$ , where  $\lambda_L$  is the excited lepton spin in the direction of quantization and  $\lambda_{e(\gamma)}$  the final electron (photon) helicity. It is easy to obtain the non-zero amplitudes

$$\begin{aligned} |\mathcal{M}_{++}^{(1/2)}|^2 &= \frac{2e^2}{\Lambda^2} (A + B)^2 M_{1/2}^4, \\ |\mathcal{M}_{--}^{(1/2)}|^2 &= \frac{2e^2}{\Lambda^2} (A - B)^2 M_{1/2}^4. \end{aligned} \quad (A3)$$

For the decay of a spin- $\frac{3}{2}$  excited fermion, following the notation of Novaes and Spehler [24], we have

$$\begin{aligned} |\mathcal{M}_{++;+-}^{(3/2)}|^2 &= \frac{e^2}{\Lambda^2} (A + B)^2 M_{3/2}^4, \\ |\mathcal{M}_{--;-+}^{(3/2)}|^2 &= \frac{e^2}{\Lambda^2} (A - B)^2 M_{3/2}^4. \end{aligned} \quad (A4)$$

In the reaction  $e(p^\mu)\gamma(q^\mu) \rightarrow e(k^\mu)\gamma(l^\mu)$ , we denote the square of the amplitudes for the exchange of a spin- $\frac{1}{2}$  (spin- $\frac{3}{2}$ ) excited fermion by  $|\mathcal{M}_{\lambda_e\lambda_\gamma\lambda'_e\lambda'_\gamma}^{(1/2,3/2)}|^2$ , where  $\lambda_{e(\gamma)}$  is the initial and  $\lambda'_{e(\gamma)}$  the final electron and (photon) helicity. The Mandelstam's variables are defined as

$$s = (p+q)^2, \quad t = (p-k)^2, \quad u = (p-l)^2. \quad (\text{A5})$$

For the exchange of a spin- $\frac{1}{2}$  excited fermion we have

$$\begin{aligned} |\mathcal{M}_{++++}^{(1/2)}|^2 &= -4e^4 \left[ \frac{s}{u} - \frac{2(A+B)^2}{\Lambda^2} \frac{s^2 (s - M_{1/2}^2)}{(s - M_{1/2}^2)^2 + (M_{1/2}\Gamma_{1/2})^2} \right. \\ &\quad \left. + \frac{(A+B)^4}{\Lambda^4} \frac{s^3 u}{(s - M_{1/2}^2)^2 + (M_{1/2}\Gamma_{1/2})^2} \right], \\ |\mathcal{M}_{++--}^{(1/2)}|^2 &= -4e^4 \frac{t (A^2 - B^2)^2 M_{1/2}^2}{\Lambda^4} \\ &\quad \times \frac{\left[ s(u - M_{1/2}^2) + u(s - M_{1/2}^2) \right]^2 + (u M_{1/2}\Gamma_{1/2})^2}{\left[ (s - M_{1/2}^2)^2 + (M_{1/2}\Gamma_{1/2})^2 \right] (u - M_{1/2}^2)^2}, \\ |\mathcal{M}_{+-+-}^{(1/2)}|^2 &= -4e^4 \left[ \frac{u}{s} - \frac{2(A+B)^2}{\Lambda^2} \frac{u^2}{u - M_{1/2}^2} + \frac{(A+B)^4}{\Lambda^4} \frac{u^3 s}{(u - M_{1/2}^2)^2} \right], \\ |\mathcal{M}_{-+-+}^{(1/2)}|^2 &= -4e^4 \left[ \frac{u}{s} - \frac{2(A-B)^2}{\Lambda^2} \frac{u^2}{u - M_{1/2}^2} + \frac{(A-B)^4}{\Lambda^4} \frac{u^3 s}{(u - M_{1/2}^2)^2} \right], \\ |\mathcal{M}_{--++}^{(1/2)}|^2 &= |\mathcal{M}_{++--}^{(1/2)}|^2, \\ |\mathcal{M}_{----}^{(1/2)}|^2 &= -4e^4 \left[ \frac{s}{u} - \frac{2(A-B)^2}{\Lambda^2} \frac{s^2 (s - M_{1/2}^2)}{(s - M_{1/2}^2)^2 + (M_{1/2}\Gamma_{1/2})^2} \right. \\ &\quad \left. + \frac{(A-B)^4}{\Lambda^4} \frac{s^3 u}{(s - M_{1/2}^2)^2 + (M_{1/2}\Gamma_{1/2})^2} \right]. \end{aligned} \quad (\text{A6})$$

In the case of spin- $\frac{3}{2}$  excited fermion we obtain

$$\begin{aligned} |\mathcal{M}_{++++}^{(3/2)}|^2 &= -4e^4 \left[ \frac{s}{u} - \frac{2(C+D)^2}{\Lambda^2} \frac{s^2}{6M_{3/2}^2} \frac{u + 2M_{3/2}^2}{u - M_{3/2}^2} \right. \\ &\quad \left. + \frac{(C+D)^4}{\Lambda^4} \frac{s^3 u}{36M_{3/2}^4} \frac{(u + 2M_{3/2}^2)^2}{(u - M_{3/2}^2)^2} \right], \end{aligned}$$

$$\begin{aligned}
|\mathcal{M}_{++--}^{(3/2)}|^2 &= -4e^4 \frac{(C^2 - D^2)^2}{\Lambda^4} \frac{t^3}{9M_{3/2}^2}, \\
|\mathcal{M}_{+-+-}^{(3/2)}|^2 &= -4e^4 \left[ \frac{u}{s} - \frac{2(C+D)^2}{\Lambda^2} \frac{u^2}{6M_{3/2}^2} \frac{(s+2M_{3/2}^2)(s-M_{3/2}^2)}{(s-M_{3/2}^2)^2 + (M_{3/2}\Gamma_{3/2})^2} \right. \\
&\quad \left. + \frac{(C+D)^4}{\Lambda^4} \frac{u^3 s}{36M_{3/2}^4} \frac{(s+2M_{3/2}^2)^2}{(s-M_{3/2}^2)^2 + (M_{3/2}\Gamma_{3/2})^2} \right], \\
|\mathcal{M}_{+--+}^{(3/2)}|^2 &= -4e^4 \frac{(C^2 - D^2)^2}{\Lambda^4} \frac{M_{3/2}^2 t^3}{4} \frac{(t+2M_{3/2}^2)^2 + (M_{3/2}\Gamma_{3/2})^2}{[(s-M_{3/2}^2)^2 + (M_{3/2}\Gamma_{3/2})^2] (u-M_{3/2}^2)^2}, \\
|\mathcal{M}_{-++-}^{(3/2)}|^2 &= |\mathcal{M}_{+-+-}^{(3/2)}|^2, \\
|\mathcal{M}_{-+-+}^{(3/2)}|^2 &= -4e^4 \left[ \frac{u}{s} - \frac{2(C-D)^2}{\Lambda^2} \frac{u^2}{6M_{3/2}^2} \frac{(s+2M_{3/2}^2)(s-M_{3/2}^2)}{(s-M_{3/2}^2)^2 + (M_{3/2}\Gamma_{3/2})^2} \right. \\
&\quad \left. + \frac{(C-D)^4}{\Lambda^4} \frac{u^3 s}{36M_{3/2}^4} \frac{(s+2M_{3/2}^2)^2}{(s-M_{3/2}^2)^2 + (M_{3/2}\Gamma_{3/2})^2} \right], \\
|\mathcal{M}_{--++}^{(3/2)}|^2 &= |\mathcal{M}_{++--}^{(3/2)}|^2, \\
|\mathcal{M}_{----}^{(3/2)}|^2 &= -4e^4 \left[ \frac{s}{u} - \frac{2(C-D)^2}{\Lambda^2} \frac{s^2}{6M_{3/2}^2} \frac{u+2M_{3/2}^2}{u-M_{3/2}^2} \right. \\
&\quad \left. + \frac{(C-D)^4}{\Lambda^4} \frac{s^3 u}{36M_{3/2}^4} \frac{(u+2M_{3/2}^2)^2}{(u-M_{3/2}^2)^2} \right]. \tag{A7}
\end{aligned}$$

For the reaction  $e^+(p^\mu)e^-(q^\mu) \rightarrow \gamma(k^\mu)\gamma(l^\mu)$ , we denote the square of the amplitudes for the exchange of a spin- $\frac{1}{2}$  and spin- $\frac{3}{2}$  excited fermion by  $|\mathcal{M}_{\lambda_{e+}\lambda_{e-}\lambda_\gamma\lambda_\gamma}^{(1/2,3/2)}|^2$ , where  $\lambda_{e^+(e^-)(\gamma)}$  is the positron(electron)(photon) helicity. The Mandelstam's variables are defined as before.

For the exchange of a spin- $\frac{1}{2}$  excited fermion, we have

$$\begin{aligned}
|\mathcal{M}_{++--}^{(1/2)}|^2 &= 4e^4 \frac{(A^2 - B^2)^2}{\Lambda^4} M_{1/2}^2 s \left[ \frac{t^2}{(t-M_{1/2}^2)^2} + \frac{u^2}{(u-M_{1/2}^2)^2} \right. \\
&\quad \left. + \frac{2ut}{(u-M_{1/2}^2)(t-M_{1/2}^2)} \right], \\
|\mathcal{M}_{+-+-}^{(1/2)}|^2 &= 4e^4 \left[ \frac{t}{u} - \frac{2(A-B)^2}{\Lambda^2} \frac{t^2}{t-M_{1/2}^2} + \frac{(A-B)^4}{\Lambda^4} \frac{ut^3}{(t-M_{1/2}^2)^2} \right], \\
|\mathcal{M}_{+--+}^{(1/2)}|^2 &= 4e^4 \left[ \frac{u}{t} - \frac{2(A-B)^2}{\Lambda^2} \frac{u^2}{u-M_{1/2}^2} + \frac{(A-B)^4}{\Lambda^4} \frac{tu^3}{(u-M_{1/2}^2)^2} \right],
\end{aligned}$$

$$\begin{aligned}
|\mathcal{M}_{-++-}^{(1/2)}|^2 &= 4e^4 \left[ \frac{t}{u} - \frac{2(A+B)^2}{\Lambda^2} \frac{t^2}{t - M_{1/2}^2} + \frac{(A-B)^4}{\Lambda^4} \frac{ut^3}{(t - M_{1/2}^2)^2} \right], \\
|\mathcal{M}_{-+-+}^{(1/2)}|^2 &= 4e^4 \left[ \frac{u}{t} - \frac{2(A+B)^2}{\Lambda^2} \frac{u^2}{u - M_{1/2}^2} + \frac{(A-B)^4}{\Lambda^4} \frac{tu^3}{(u - M_{1/2}^2)^2} \right], \\
|\mathcal{M}_{--++}^{(1/2)}|^2 &= |\mathcal{M}_{++--}^{(1/2)}|^2,
\end{aligned} \tag{A8}$$

and for the spin- $\frac{3}{2}$  exchange we have

$$\begin{aligned}
|\mathcal{M}_{++++}^{(3/2)}|^2 &= 4e^4 \frac{(C^2 - D^2)^2}{\Lambda^4} \frac{M_{3/2}^2 s^3}{4} \left[ \frac{1}{(t - M_{3/2}^2)^2} + \frac{1}{(u - M_{3/2}^2)^2} \right. \\
&\quad \left. + \frac{2}{(t - M_{3/2}^2)(u - M_{3/2}^2)} \right], \\
|\mathcal{M}_{++--}^{(3/2)}|^2 &= 4e^4 \frac{(C^2 - D^2)^2}{\Lambda^4} \frac{s^3}{9M_{3/2}^2}, \\
|\mathcal{M}_{+-+-}^{(3/2)}|^2 &= 4e^4 \left[ \frac{t}{u} - \frac{2(C-D)^2}{\Lambda^2} \frac{u^2(t + 2M_{3/2}^2)}{6M_{3/2}^2(t - M_{3/2}^2)} \right. \\
&\quad \left. + \frac{(C-D)^4}{\Lambda^4} \frac{u^3t(t + 2M_{3/2}^2)^2}{36M_{3/2}^4(t - M_{3/2}^2)^2} \right], \\
|\mathcal{M}_{+-+-}^{(3/2)}|^2 &= 4e^4 \left[ \frac{t}{u} - \frac{2(C-D)^2}{\Lambda^2} \frac{t^2(u + 2M_{3/2}^2)}{6M_{3/2}^2(u - M_{3/2}^2)} \right. \\
&\quad \left. + \frac{(C-D)^4}{\Lambda^4} \frac{t^3u(u + 2M_{3/2}^2)^2}{36M_{3/2}^4(u - M_{3/2}^2)^2} \right], \\
|\mathcal{M}_{-+-+}^{(3/2)}|^2 &= 4e^4 \left[ \frac{u}{t} - \frac{2(C+D)^2}{\Lambda^2} \frac{u^2(t + 2M_{3/2}^2)}{6M_{3/2}^2(t - M_{3/2}^2)} \right. \\
&\quad \left. + \frac{(C+D)^4}{\Lambda^4} \frac{u^3t(t + 2M_{3/2}^2)^2}{36M_{3/2}^4(t - M_{3/2}^2)^2} \right], \\
|\mathcal{M}_{-++-}^{(3/2)}|^2 &= 4e^4 \left[ \frac{t}{u} - \frac{2(C+D)^2}{\Lambda^2} \frac{t^2(u + 2M_{3/2}^2)}{6M_{3/2}^2(u - M_{3/2}^2)} \right. \\
&\quad \left. + \frac{(C+D)^4}{\Lambda^4} \frac{t^3u(u + 2M_{3/2}^2)^2}{36M_{3/2}^4(u - M_{3/2}^2)^2} \right], \\
|\mathcal{M}_{--++}^{(3/2)}|^2 &= |\mathcal{M}_{++--}^{(3/2)}|^2, \\
|\mathcal{M}_{----}^{(3/2)}|^2 &= |\mathcal{M}_{++++}^{(3/2)}|^2.
\end{aligned} \tag{A9}$$

It is interesting to notice that for right-handed and left-handed couplings of the excited

fermion the amplitudes (A8) and (A9) with equal electron and positron helicity receive no contribution from QED or from the excited states. This was expected since we have neglected the external fermion masses (electron and positron).

## REFERENCES

[1] See, for instance, D. Schaile, *Precision Tests of the Electroweak Interaction*, plenary talk (Pl-2) presented at the 27th International Conference on High Energy Physics, Glasgow, Scotland, July 1994.

[2] For review and references see:  
H. Harari, Phys. Reports, **104**, 159 (1984);  
W. Buchmüller, Acta Phys. Austriaca, Suppl. XXVII, 517 (1985);  
M. E. Peskin, Proceedings of the 1985 International Symposium on Lepton and Photon Interactions at High Energies, Kyoto, (Kyoto Univ., Kyoto, 1985), edited by M. Konuma and K. Takahashi, p. 714;  
M. Suzuki, “Survey of Composite Particle Models of Electroweak Interaction”, Proceedings International Symposium on Bound Systems and Extended Objects, Karuizawa, Japan, March, 1992 (preprint UCB-PTH-92-17, May 1992).

[3] ALEPH Collaboration, D. Decamp *et al.* Phys. Lett. **B236**, 501 (1990);  
L3 Collaboration, B. Adeva *et al.* Phys. Lett. **B247**, 177 (1990); **B250**, 199 (1990); **B250**, 205 (1990); O. Adriani *et al.*, Phys. Lett. **B288**, 404 (1992).  
OPAL Collaboration, M. Z. Akrawy *et al.* Phys. Lett. **B240**, 497 (1990); **B244**, 135 (1990); **B257**, 531 (1991);  
DELPHI Collaboration, P. Abreu *et al.*, Phys. Lett. **B268**, 296 (1991); Z. Phys. **C53**, 41 (1992).  
For a review of the LEP results see: ALEPH Collaboration, D. Decamp *et al.*, Phys. Rep. **216**, 253 (1992); L3 Collaboration, O. Adriani *et al.*, Phys. Rep. **236**, 1 (1993);

[4] H1 Collaboration, I. Abt *et al.*, Nucl. Phys. **bf B396**, 3 (1993);  
ZEUS Collaboration, M. Derrick *et al.*, Phys. Lett. **B316**, 207 (1993).

[5] K. Enqvist and J. Maalampi, Phys. Lett. **B135**, 329 (1984).

[6] J. Kühn and P. Zerwas, Phys. Lett. **B147**, 189 (1984).

[7] N. Cabibbo, L. Maiani, and Y. Srivastava, Phys. Lett. **B139**, 459 (1984);  
 F. A. Berends and P. H. Daverveldt, Nucl. Phys. **B272**, 131 (1986);  
 A. Feldmaier, H. Salecker, and F. C. Simm, Phys. Lett. **B223**, 234 (1989);  
 M. Martinez, R. Miquel, and C. Mana, Z. Phys. **C46**, 637 (1990);  
 F. Boudjema and A. Djouadi, Phys. Lett. **B240**, 485 (1990);  
 Maria Bardadin–Otwinowska, Z. Phys. **C55**, 163 (1992);  
 J. C. Montero and V. Pleitez, Phys. Lett. **B321**, 267 (1994).

[8] K. Hagiwara, S. Komamiya, and D. Zeppenfeld, Z. Phys. **C29**, 115 (1985).

[9] F. Boudjema, A. Djouadi, and J. L. Kneur, Z. Phys. **C57**, 425 (1993).

[10] I. F. Ginzburg and D. Yu. Ivanov, Phys. Lett. **B276**, 214 (1992);  
 T. Kon, I. Ito and Y. Chikashige, Phys. Lett. **B287**, 277 (1992);  
 E. Boos, A. Pukhov, and A. Beliaev, Phys. Lett. **B296**, 452 (1992).

[11] R. B. Palmer, Ann. Rev. Nucl. Part. Sci. **40**, 529 (1990).

[12] F. R. Arutyunian and V. A. Tumanian, Phys. Lett. **4**, 176 (1963);  
 R. H. Milburn, Phys. Rev. Lett. **10**, 75 (1963);  
 I. F. Ginzburg, G. L. Kotkin, V. G. Serbo, and V. I. Telnov, Nucl. Instrum. Methods **205**, 47 (1983);  
 V. I. Telnov, Nucl. Instrum. Methods **A294**, 72 (1990).

[13] I. F. Ginzburg, G. L. Kotkin, V. G. Serbo, and V. I. Telnov, Nucl. Instrum. Methods **219**, 5 (1984).

[14] F. M. Renard, Phys. Lett. **B116**, 264 (1982).

[15] N. Cabibbo, L. Maiani, and Y. Srivastava, Phys. Lett. **B139**, 459 (1984).

[16] F. E. Low, Phys. Rev. Lett. **14**, 238 (1965).

[17] W. Rarita and J. Schwinger, Phys. Rev. **60**, 61 (1941);

Ph. Salin, Nuovo Cimento **32**, 521 (1964).

[18] J. Leite Lopes, J. A. M. Simões and D. Spehler, Phys. Lett. **B94**, 367 (1980); Phys. Rev. **D23**, 797 (1981); Phys. Rev. **D25**, 1854 (1982);  
 D. Spehler, O. J. P. Éboli, G. C. Marques, A. A. Natale and S. F. Novaes, Phys. Rev. **D36**, 1358 (1987).

[19] R. G. Ellis, M. Matsuda, and B. H. J. McKellar, Phys. Rev. **D32**, 1657 (1985).

[20] F. M. Renard, Phys. Lett. **B139**, 449 (1984);  
 M. Suzuki, Phys. Lett. **B143**, 237 (1984).

[21] Of course, in a linear collider one can always work with two electron beams, making it easier to obtain high luminosity polarized beams.

[22] We should notice that, for  $M_{1/2(3/2)} > s$ , the interference term, that is proportional to  $1/\Lambda^2$ , flips its sign, leading to a change in the sign of the deviations  $\delta_{e,\gamma}$ .

[23] F. A. Berends and W. T. Giele, Nucl. Phys. **B294**, 700 (1987).

[24] S. F. Novaes and D. Spehler, Nucl. Phys. **B371**, 618 (1992).

[25] We take this opportunity to correct some misprints in Eq. (30) of Ref. [24].

## FIGURES

FIG. 1. (a) Luminosity of backscattered photons in a  $e^- \gamma$  collider as a function of the center-of-mass energy ( $E_{\text{cm}}$ ). We assumed  $\sqrt{s} = 500$  GeV,  $\zeta = 4.83$ , and  $P_e \cdot P_l = 0$  (solid),  $P_e \cdot P_l = -0.9$  (dots), and  $P_e \cdot P_l = 0.9$  (dashes). (b) Plot of  $\xi_2$  as function of  $E_{\text{cm}}$  for  $\sqrt{s} = 500$  GeV,  $P_e = 0.9$ , and  $P_l = 0$  (solid),  $-1$  (dots), and  $1$  (dashes).

FIG. 2. Invariant mass distribution for the process (12), for the exchange of spin- $\frac{1}{2}$  (dashes) and spin- $\frac{3}{2}$  (dots) excited fermions both with mass  $M_{1/2(3/2)} = 250$  GeV at  $\sqrt{s} = 500$  GeV with unpolarized beams. We considered coupling strengths that lead to deviations of  $3\sigma$  in the total cross section with respect to the standard model prediction (solid).

FIG. 3. (a) Discovery contour for LH excited states of spin- $\frac{1}{2}$  for  $\sqrt{s} = 500$  GeV and  $\mathcal{L} = 10$   $\text{fb}^{-1}$ . The dotted line corresponds to  $P_e = -0.9$ ,  $P_p = -0.9$ , and  $P_l = 1$  while the dashed one stands for  $P_e = -0.9$ ,  $P_p = -0.9$ , and  $P_l = -1$ . (b) The same as (a) for LH spin- $\frac{3}{2}$  where the dotted line corresponds to  $P_e = -0.9$ ,  $P_p = 0.9$ , and  $P_l = -1$  and the dashed one to  $P_e = -0.9$ ,  $P_p = 0.9$ , and  $P_l = 1$ . In both figures, the solid lines stand for unpolarized beams. By taking the opposite of all polarizations, the same discovery contours are valid for RH couplings.

FIG. 4. (a) Deviation  $\delta_e$  [Eq. (16)], at  $\sqrt{s} = 500$  GeV, for LH spin- $\frac{1}{2}$  (solid), RH spin- $\frac{1}{2}$  (dashes), LH spin- $\frac{3}{2}$  (dots), and RH spin- $\frac{3}{2}$  (dotdash) excited states as function of its mass for  $P_e = 0.9$  and unpolarized backscattered photons. (b) Deviation  $\delta_\gamma$  [Eq. (17)] for unpolarized electron and laser beams and a positron beam with  $P_p = 0.9$ . In both figures, these deviations have a statistical significance of  $3\sigma$ .

FIG. 5. Angular distribution for the process  $e^+e^- \rightarrow \gamma\gamma$ , where  $\theta$  is the angle between the incoming electron and the outgoing photon. We assumed unpolarized beams and  $\sqrt{s} = 500$  GeV. We chose the values of  $\Lambda$  that lead to  $3\sigma$  deviations from the standard model prediction for the total cross section. The background is represented by the solid line and the spin- $\frac{1}{2}$  ( $\frac{3}{2}$ ) exchange is represented by the dotted (dashed) line. We performed an angular cut of  $5^\circ$  on the polar angle with respect to the beam pipe.

FIG. 6. Left-right asymmetry factor  $\mathcal{A}_{LR}$ , at  $\sqrt{s} = 500$  GeV, for LH spin- $\frac{1}{2}$  (solid), RH spin- $\frac{1}{2}$  (dashes), LH spin- $\frac{3}{2}$  (dots), and RH spin- $\frac{3}{2}$  (dotdash) excited states as function of their masses, for  $P_e = 0.9$  and  $P_p = 0$ .

FIG. 7. Discovery regions for LEP II. The limits for the spin- $\frac{1}{2}$  ( $\frac{3}{2}$ ) excited state is represented by the solid (dotted) line for  $\sqrt{s} = 175$  GeV with  $\mathcal{L} = 500 \text{ pb}^{-1}$ , and by the dashed (dotdashed) one for  $\sqrt{s} = 205$  GeV with  $\mathcal{L} = 300 \text{ pb}^{-1}$ . We performed an angular cut of  $12^\circ$  in the polar angle of the final state photons.

FIG. 8. Comparison of the discovery regions for  $e^+e^-$  (dashed) and  $e^-\gamma$  (solid) operating modes with unpolarized beams, at  $\sqrt{s} = 500$  GeV. The figure a (b) shows the discovery regions for spin- $\frac{1}{2}$  ( $\frac{3}{2}$ ) excited states.

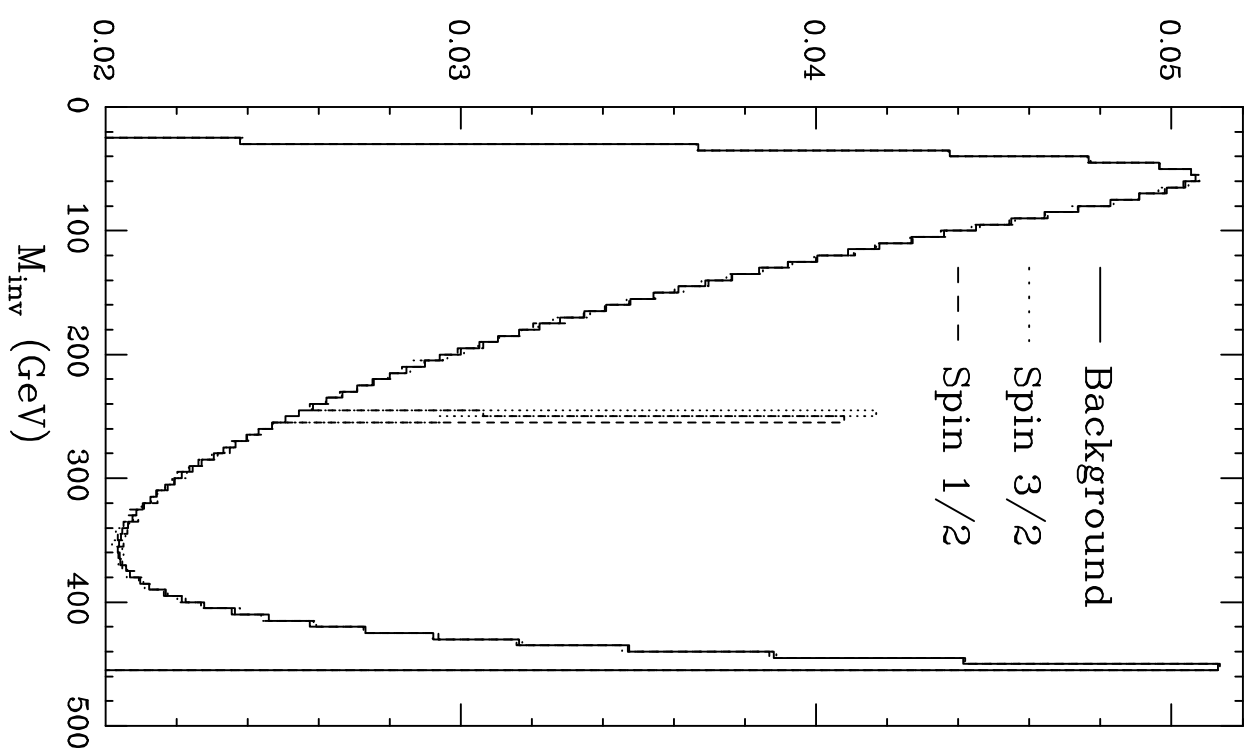
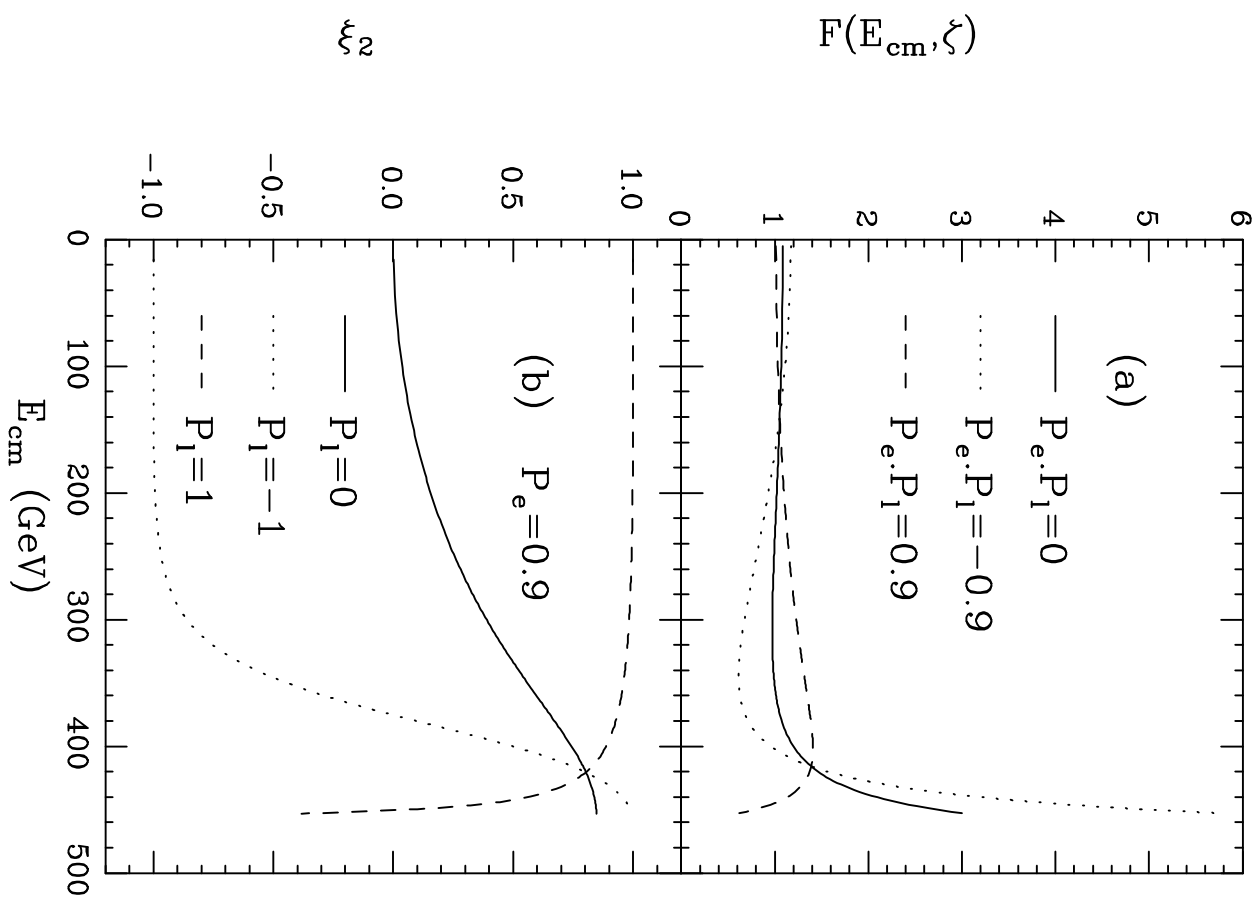


Figure 1

Figure 2

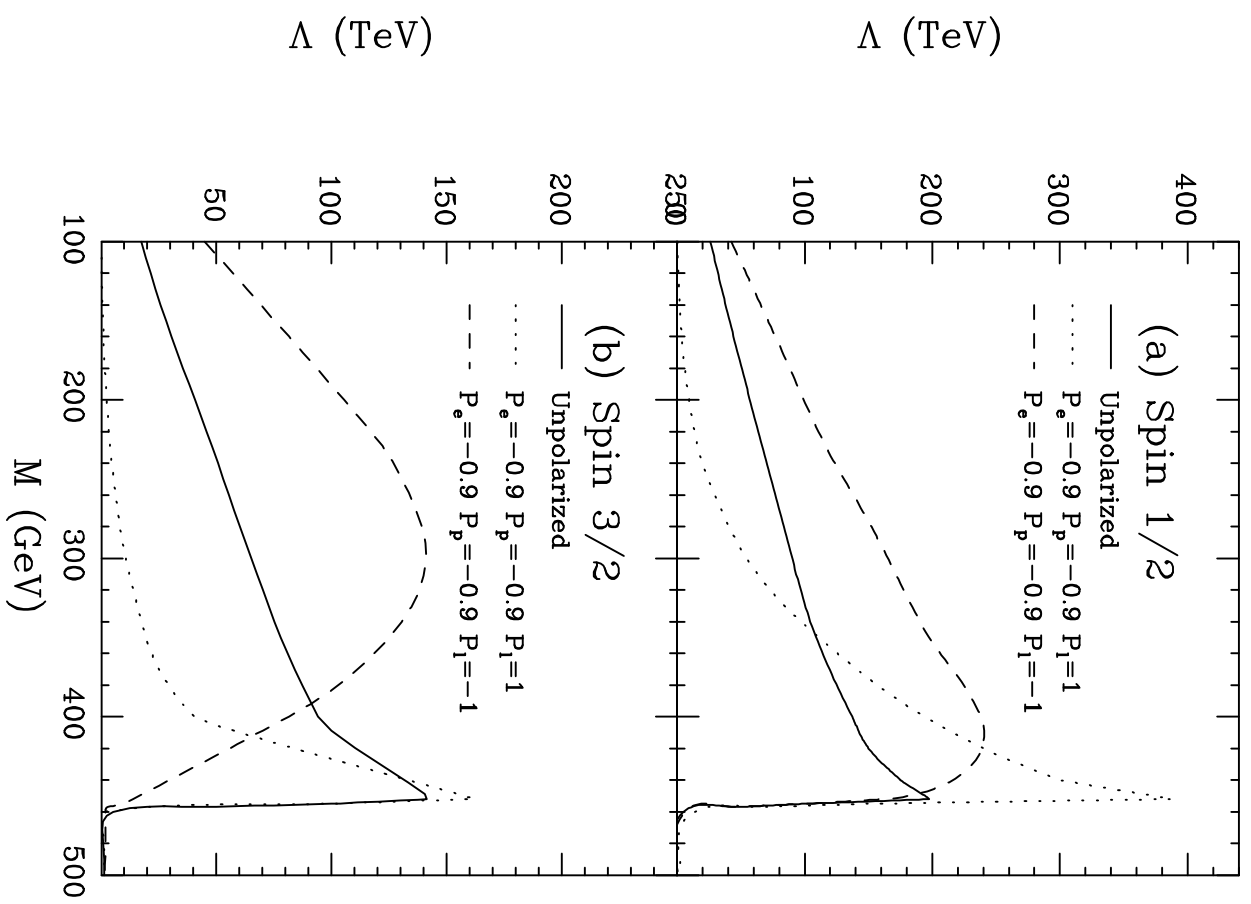


Figure 3

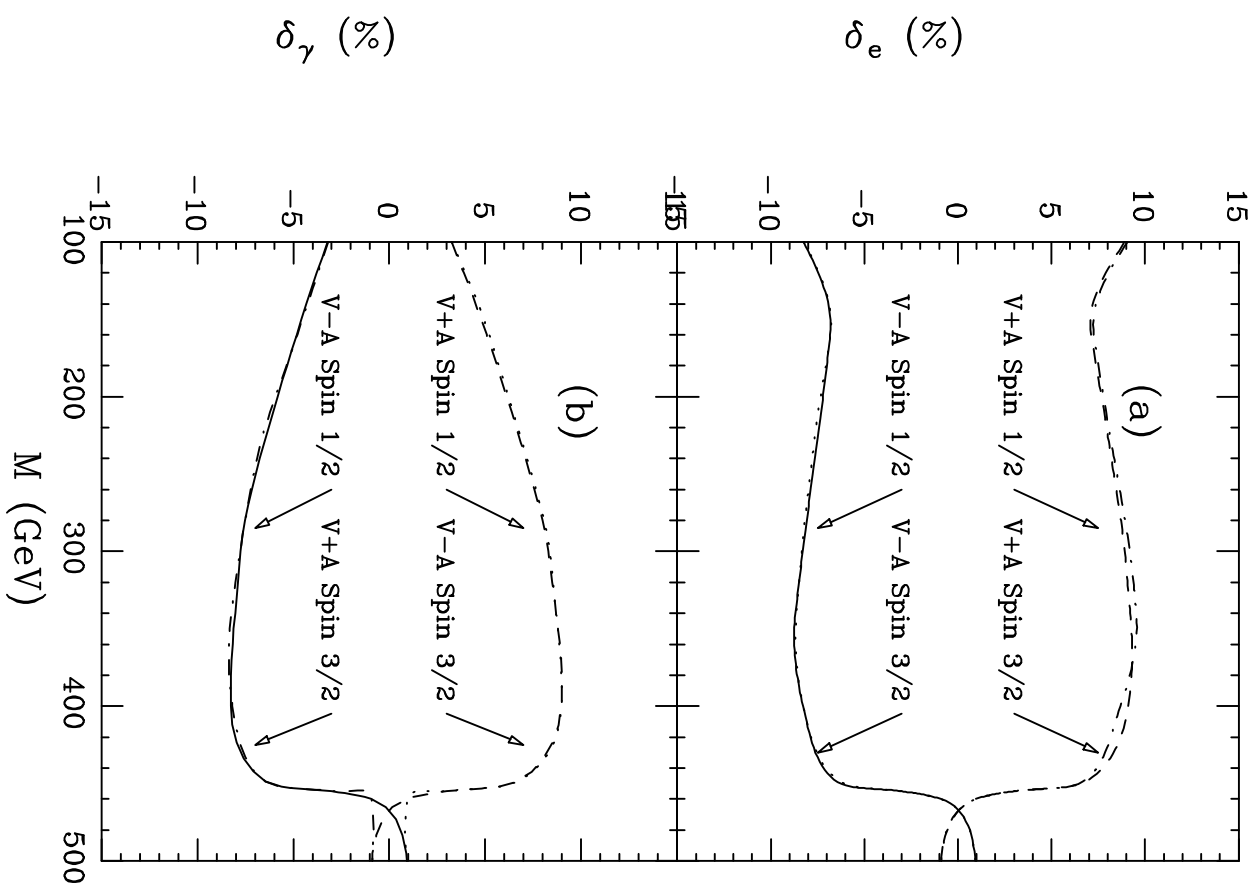


Figure 4

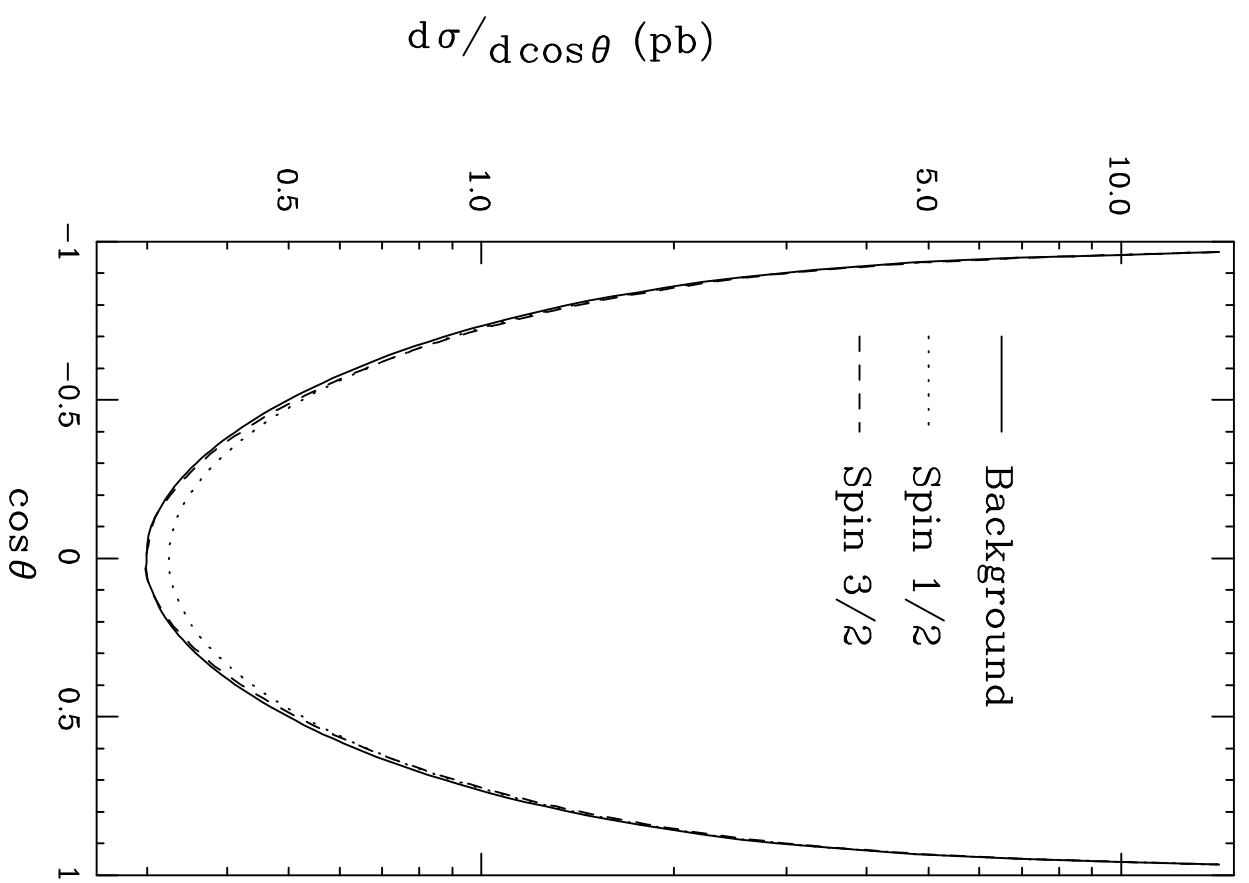


Figure 5

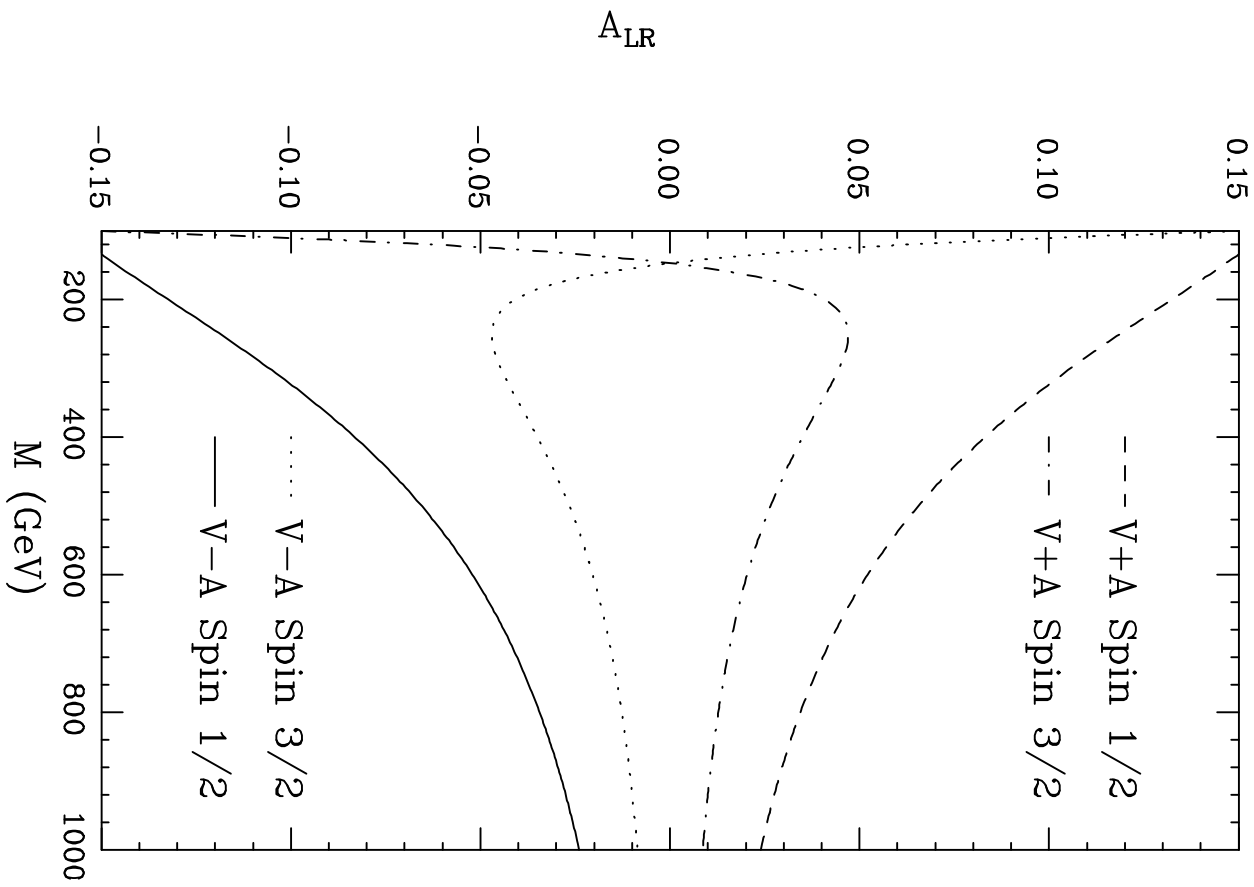


Figure 6

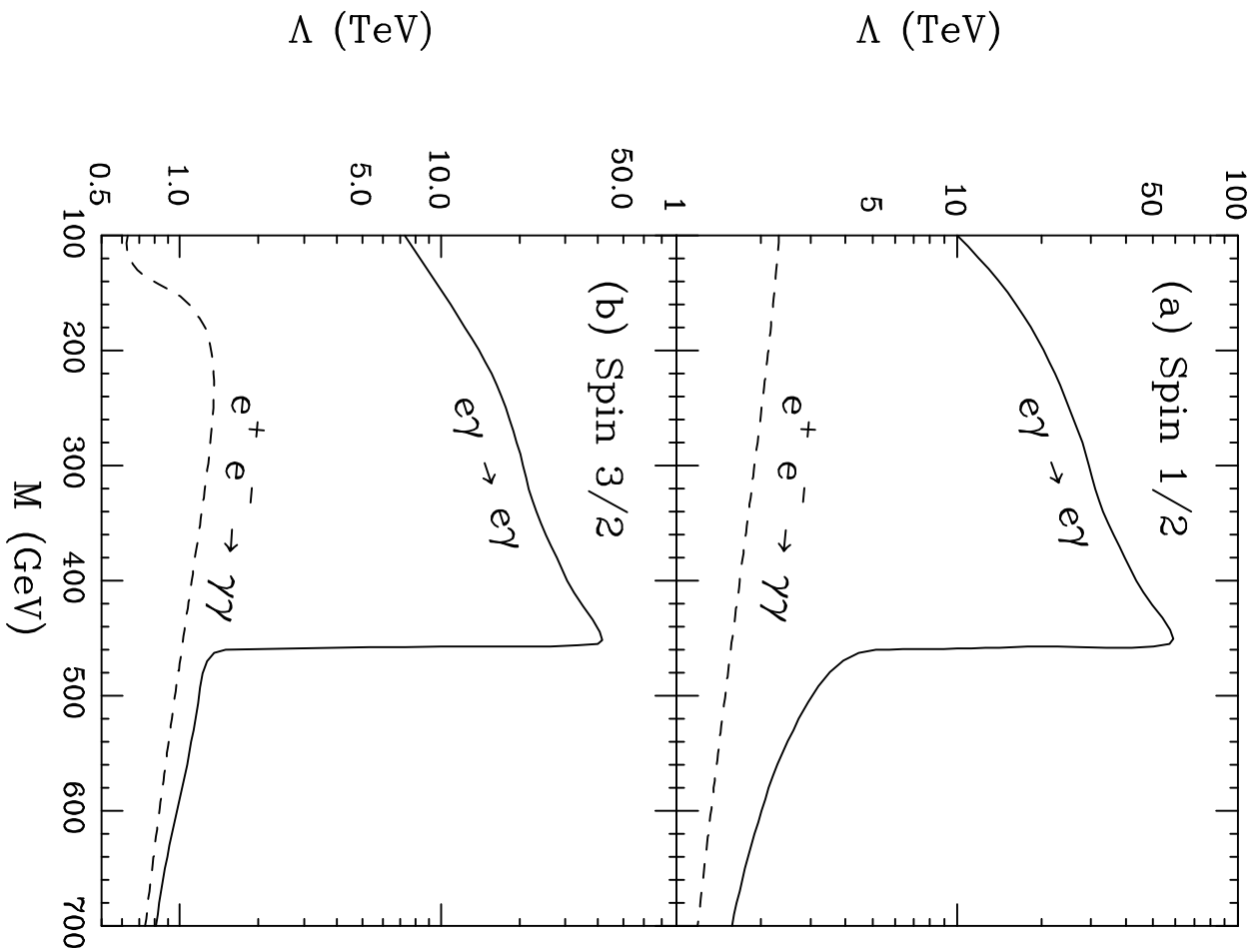
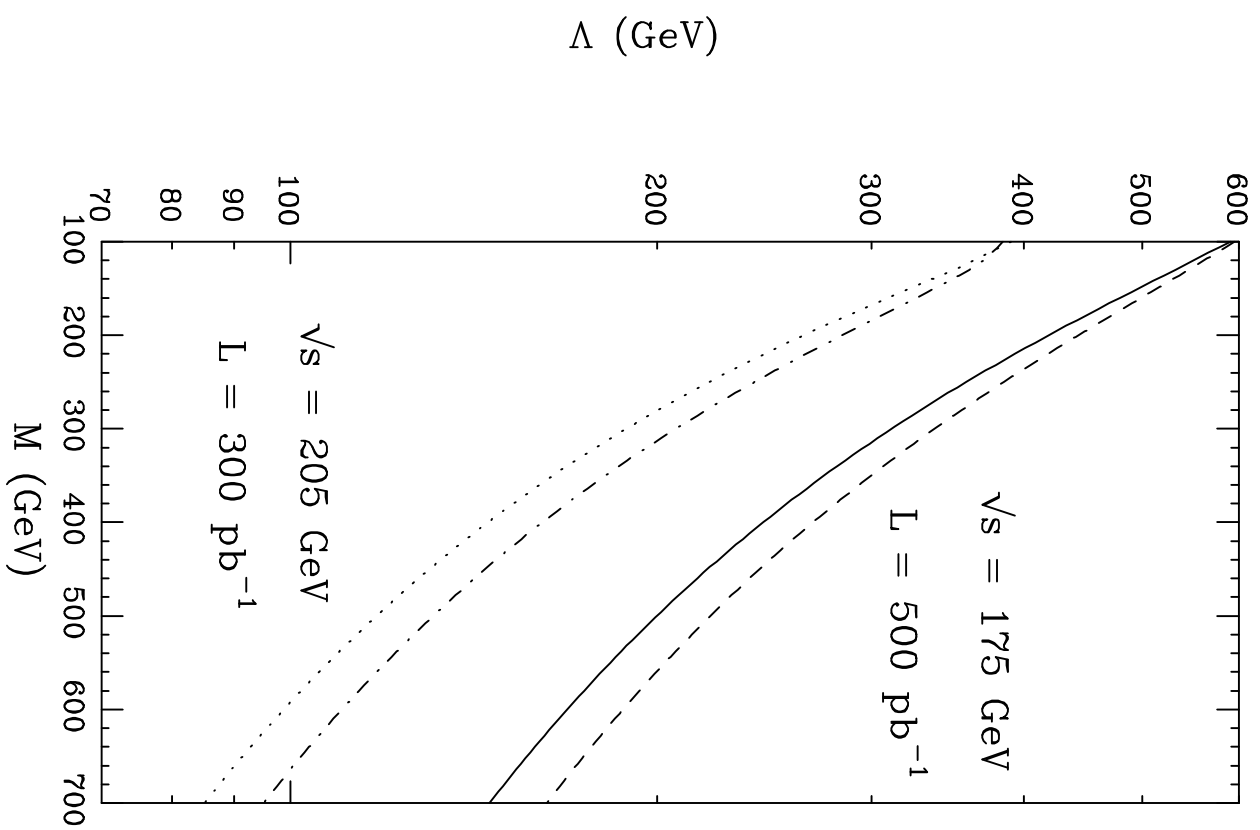


Figure 7

Figure 8